Malaysian Journal of Chemistry, 2025, Vol. 27(3), 20-30
(Special Issue: *2nd International Science and Technology Colloquium, i-COSTECH 2024*)

Tetracycline Degradation Over $CuWO_4$ Photocatalyst under Low-Power Visible Light Irradiation

Minh-Vien Le[1,2]*, Le-Thuy-Hien Doan[1,2], Ngoc-Diem-Trinh Huynh[1,2], Trung-Tan Tran[1,2], Manh Thang Ngo[1,2], Van Hoang Luan[1,2], Suresh Sagadevan[3], Abu Hassan Nordin[4], Zuliahani Ahmad[5] and Phan Thi Que Phuong[6]

[1]Faculty of Chemical Engineering, Ho Chi Minh City University of Technology (HCMUT), Ho Chi Minh City, Vietnam
[2]Vietnam National University Ho Chi Minh City, Ho Chi Minh City, Vietnam
[3]Nanotechnology & Catalysis Research Centre (NANOCAT), Institute for Advanced Studies (IAS), University of Malaya (UM), Level 3, Block A, 50603 Kuala Lumpur, Malaysia
[4]Faculty of Applied Sciences, Universiti Teknologi MARA (UiTM), Arau 02600, Perlis, Malaysia
[5]Faculty of Applied Sciences, Universiti Teknologi MARA Cawangan Perlis, Kampus Arau, 02600 Arau,Perlis, Malaysia
[6]Institute of Advanced Technology, Viet Nam Academy of Science and Technology, Ho Chi Minh City, 700000, Vietnam
*Corresponding author (e-mail: lmvien@hcmut.edu.vn)

$CuWO_4$ materials were successfully prepared using a combination of hydrothermal and calcination methods under various conditions and characterized through multiple techniques. The influence of synthesis conditions on the physicochemical properties and photocatalytic degradation of tetracycline (TC) using the $CuWO_4$ catalyst were systematically investigated. The samples subjected to 24–hour hydrothermal treatment at 200 °C followed by calcination at 500 °C exhibited the highest photodegradation efficiency, achieving a rate constant of 1.24×10^{-2} min^{-1}. Notably, the prepared samples demonstrated the ability to perform photocatalytic reactions over a broad pH range of 3.0 to 10.0. Reactive species such as $\bullet O_2^-$, h^+ and •OH were found to contribute to TC degradation, with photo-generated h^+ identified as the dominant species. This study presents an effective approach to enhancing the photocatalytic performance of $CuWO_4$-based catalysts for antibiotic degradation in wastewater treatment applications.

Keywords: Antibiotic degradation; $CuWO_4$; tetracycline

Received: September 2024; Accepted: December 2024

Pollution caused by human activities and rapid industrial growth is giving rise to significant environmental threats [1]. A particularly concerning trend is the upward concentration of antibiotics in water sources. The persistence of these antibiotics in aquatic environments can disrupt the balance of microorganisms, potentially affecting the food chain and the overall health of the entire ecosystem. Additionally, antibiotic residues in water may foster the emergence of antibiotic resistance genes (ARGs) and antibiotic-resistant bacteria (ARB) [2], leading to the spread of resistance within microbial communities, which could complicate the treatment of bacterial infections and pose notable challenges to public health and environmental safety.

In recent years, various strategies have been explored for the removal of antibiotic pollutants from water sources, with photocatalytic degradation emerging as a highly promising technique. The use of nanoscale semiconductor oxide photocatalysts that harness sunlight has gained global attention. These photocatalysts are economically viable, chemically inert, non-toxic and environmentally friendly, while also being performed under ambient conditions and offering broad applicability [1, 3]. Recent studies have highlighted that metal tungstate with the general formula AWO_4 (where A = Cu, Mn, Mg, Zn, and Cd) have attracted considerable interest from the scientific community [4-6]. These materials possess suitable bandgap energy, which provides a capable of effectively harnessing visible light for photocatalytic process, thus presenting a promising area for further investigation. Among of them, $CuWO_4$ stands out as a potential photocatalysts for real-world applications due to its narrow band gap energy (2.1–2.3 eV) and high stability against photo-corrosion [7], which allows it to effectively absorb and utilize a broad spectrum of solar light [8]. As a result, $CuWO_4$ has become an attractive option for photocatalytic materials in water purification.

Furthermore, the valence band (VB) edge position of $CuWO_4$ has been determined to be 2.41 V

†Paper presented at the 2nd International Science and Technology Colloquium (i-COSTECH 2024)

vs. NHE [9], which is more positive than that of •OH/OH^- (1.99 V vs. NHE). This characteristic enables $CuWO_4$ to produce the hydroxyl radical (•OH) more easily (Equation (1)). These •OH are highly active and can attack to degrade contaminants, breaking them down into intermediates or smaller inorganic molecules.

$$h_{VB}^{+} + OH^{-} \rightarrow \bullet OH \quad (1)$$

While the $CuWO_4$ photocatalyst offers remarkable advantages, it still faces limitations in the degradation of antibiotic degradation. Many antibiotics possess robust molecular structures, making them highly resistant to decomposition [10, 11]. Therefore, there is an urgent need to develop and design photocatalysts with enhanced activity. Doping $CuWO_4$ with foreign elements, either metallic or non-metallic, can significantly improve its performance by creating surface defects and oxygen vacancies. These oxygen vacancies are particularly crucial as they act as electron mediators, enhancing the photocatalyst's redox capability [12]. Consequently, the accumulated electrons in the conduction band (CB) of the photocatalyst react with the adsorbed oxygen molecules to generate superoxide radical anion (•O_2^-), further improving photocatalytic efficiency. In general, semiconductors photocatalysts suffer from electron-hole recombination, where photogenerated electrons and holes recombine before participating in redox reactions, reducing overall efficiency. Decorating $CuWO_4$ with graphene quantum dots (GQDs) addresses this issue by inhibiting electron–hole recombination and enhancing visible light absorption. GQDs act as electron extractors, providing conductive pathways for photogenerated electrons to migrate from $CuWO_4$. By reducing electron-hole recombination, GQDs increase the availability of charge carriers for redox reactions, significantly boosting photocatalytic performance [13].

Additionally, designing heterostructure catalyst systems is a great strategy for developing advanced photocatalysts for diverse applications. For instance, the Z-scheme $CuWO_4$/g-C_3N_4 nanocomposite improves light absorption and promotes charge separation, achieving high efficiency in the synthesis of tetrahydroindazolone derivatives [7]. Similarly, the $ZnFe_2O_4$/$CuWO_4$ heterostructure has demonstrated excellent photocatalytic activity, even under real wastewater conditions under visible light irradiation, achieving TC degradation rates that are 5.1 and 3.3 times faster than those of $ZnFe_2O_4$ and $CuWO_4$ individually [14]. Furthermore, the Z–scheme of Ag_3PO_4/$CuWO_4$ heterojunction not only improves charge separation and transportation but also extends the photocatalyst's visible-light absorption range [15]. It could be concluded that doping $CuWO_4$ with foreign elements or combining it with suitable substances can significantly enhance the photocatalytic activity of the modified-$CuWO_4$ [15]. Moreover, intrinsic properties of the catalyst, such as crystalline structure, band gap energy, band edge position, particle size, surface area and morphologies are influenced by synthetic conditions. Therefore, to further improve the photocatalytic performance of modified $CuWO_4$, it is crucial to systematically investigate the synthetic conditions employed in its preparation.

To the best of our knowledge, the influence of synthetic conditions on the photocatalytic activity of $CuWO_4$ under visible light irradiation for antibiotic degradation has not yet been systematically investigated. Previous studies have examined the effect of pH (ranging from 3 to 9) on the photocatalytic efficiency of $CuWO_4$ for TC degradation, using a constant catalyst dosage of 0.5 gL^{-1}, and proposed a photocatalytic degradation mechanism for TC by $CuWO_4$ [9]. In this study, we focus on different synthetic conditions influence the photocatalytic activity of $CuWO_4$ samples prepared via the hydrothermal method. The appropriate parameters for achieving high photocatalytic performance in TC degradation were identified. Furthermore, the effects of key treatment conditions such as catalyst dosage and solution pH, on the photocatalytic degradation of TC was systematically elucidated. The roles of active radicals in the degradation process were also examined through radical scavenging experiments, enabling the proposal of a potential TC degradation mechanism. This study provides a comprehensive understanding of $CuWO_4$ as an efficient photocatalyst and offers valuable insights for designing effective catalyst system for wastewater remediation. Additionally, this study introduces a straightforward approach to optimizing the balance between light absorption, particularly under low-power simulated sunlight (26 W), and preparation conditions to achieve superior photocatalytic degradation performance.

EXPERIMENTAL

Chemicals and Materials

Copper(II) nitrate trihydrate ($Cu(NO_3)_2.3H_2O$, 99%) and sodium tungstate dihydrate ($Na_2WO_4.H_2O$, 99.5%) were purchased from Macklin. Ethanol (C_2H_5OH, 99.5%) was sourced from CEMACO. Sodium hydroxide (NaOH, >98%), hydrochloric acid (HCl, 36.5%), tert-butanol (TBA, 99%), p-benzoquinone (p-BQ, $C_6H_4O_2$, 99%), and Tetracycline ($C_{22}H_{24}N_2O_8$.HCl, p.a) were obtained from Xilong Scientific Co., Ltd. Ammonium oxalate ($(NH_4)_2C_2O_4$, AO, 99%) was provided by GHTECH Co., Ltd. All reagents were used as received without further purification. Double distilled water (DW) was used in all experiments.

Synthesis of $CuWO_4$

$CuWO_4$ was fabricated via a hydrothermal method followed by heat treatment. In typical procedure, 2.984 g $Na_2WO_4.2H_2O$ (9.0 mmol) and 2.196 g $Cu(NO_3)_2.3H_2O$ (9.0 mmol) were dissolved separately in 30 mL of DW and stirred for 30 min. The Na_2WO_4 solution

was then added dropwise to the $Cu(NO_3)_2$ solution under vigorous stirring. The pH of the resulting mixture was adjusted to 8.0 for 1 h, then transferred into a 100 ml Teflon-lined stainless-steel autoclave and subjected to hydrothermal treatment at predetermined temperature (160, 180, 200, 220 °C) for 24 h. After naturally cooling to room temperature, the green precipitate was collected by centrifugation, washed multiple times with DW and ethanol and dried at 60 °C for 4 h. Finally, the dried samples were calcined at designated temperatures (400, 500, 600 °C) for 2 h at a ramp rate of 10 °Cmin^{-1}. The $CuWO_4$ final products were denoted as CWO-x-y, where x represents the hydrothermal temperature (160, 180, 200, 220 °C), and y indicates the calcination temperature (400, 500, 600 °C). For instance, CWO-200-500 denotes the product hydrothermally treated at 200 °C and then calcined at 500 °C.

Characterization

X-ray diffraction (XRD) patterns were obtained using a Malvern X-ray diffractometer (Panalytical), which employed a Cu-K_α radiation source (40 kV, 40 mA, λ= 0.15418 nm). The diffraction angle varied with a step size 0.01313° and a dwell time of 100 s per step. The degree of crystallinity (X_c) was calculated by measuring the intensities of the crystalline (I_c) and amorphous (I_a) components in the sample, as described by Equation (2) [16]. Scanning electron microscopy (SEM) analysis was performed on a Hitachi FE-SEM S4800 instrument. N_2 adsorption-desorption isotherms were recorded on a Quantachrome NOVA 1000E analyzer, operating in the relative pressure (P/P_0) range 0.046 – 0.350. Zeta potential was measured on a Malvern Zeta-sizer. The pH value at the material's isoelectric point (pH_{pzc}) can be calculated using Equation (3):

$$X_c = \frac{I_c}{I_a+I_c} \times 100 \quad (2)$$

$$pH = 7 - mV/57.14 \quad (3)$$

Photocatalytic Performance Test

The photocatalytic activities of the catalysts were evaluated by the degradation of TC. For each experiment, 100 mg of the catalyst was dispersed in 200 mL of TC solution with an initial concentration of 20 mgL^{-1}. The suspension was stirred continuously in darkness for 1 h to establish the adsorption–desorption equilibrium. Subsequently, the system was illuminated by a 26W Exo Terra Natural Light lamp, positioned 5 cm above the surface of the suspension for 3 h. At regular intervals, 3 mL of reaction solution was withdrawn and filtrated through a 0.45 µm nylon membrane to separate the catalyst before analyzing the remaining concentration of TC using a UV−Visible spectrophotometer. The TC degradation efficiency was calculated using the following equation (Equation (4)). where A_t is the absorbance at the time t and A_o is the absorbance of the initial TC solution (20 mgL^{-1}).

$$DR\ (\%) = \left(1 - \frac{At}{A_0}\right) 100\% \quad (4)$$

The kinetic parameters of TC decomposition, which follow pseudo-first order reaction kinetics, were determined using Equation (5), based on the Langmuir-Hinshelwood model.

$$-ln\left(\frac{C}{C_0}\right) = kt \quad (5)$$

Where C and C_0 represent the concentration of TC at a given treatment time and the initial concentration at t = 0 during irradiation, respectively. The symbol k denotes the apparent pseudo-first-order rate constant.

The photocatalytic degradation mechanism of TC was elucidated based on the result of radical trapping experiments. Different scavengers such as BQ (0.1 mM), TBA (0.5 M) and AO (1.0 mM) were added into the suspension to quench $\bullet O_2^-$, •OH, and hole (h^+), respectively.

RESULTS AND DISCUSSION

Characteristics of the Prepared $CuWO_4$

The crystallinity and phase integrity of the samples were analyzed using XRD technique. **Figure 1** displays the XRD patterns of $CuWO_4$ samples prepared at different calcination (a) and hydrothermal temperature **(b)**. **Figure 1(a)** displays the XRD patterns of $CuWO_4$ samples that were underwent hydrothermal treatment at 200 °C followed by calcination at various temperatures. It can be seen that the XRD pattern of the sample calcined at 400 °C contains characteristic peaks for both the monoclinic $CuWO_4.2H_2O$ (JCPDS No 33–0503) and triclinic $CuWO_4$ (JCPDS No 88–0269) crystalline phases [17-19]. At higher calcined temperature, both samples calcined at 500 °C and 600 °C resulted peaks characterizing the triclinic $CuWO_4$ crystalline phase only, with peaks at 15.3°, 19.0°, 22.9°, 23.5°, 24.0°, 25.9°, 28.7°, 30.1°, 31.6°, 32.1° and 35.6°, corresponding to the (010), (100), (110), (0$\bar{1}$1), (011), ($\bar{1}$01), ($\bar{1}\bar{1}$1), (111), (020), ($\bar{1}$11) and (1$\bar{1}$1) crystal planes, respectively. No impurity phases were detected. The XRD pattern of samples calcined at 600 °C presents the higher intensity peaks. The correspondingly higher peak intensities in XRD pattern of the sample calcined at 600 °C indicates higher crystallinity of these prepared samples [20].

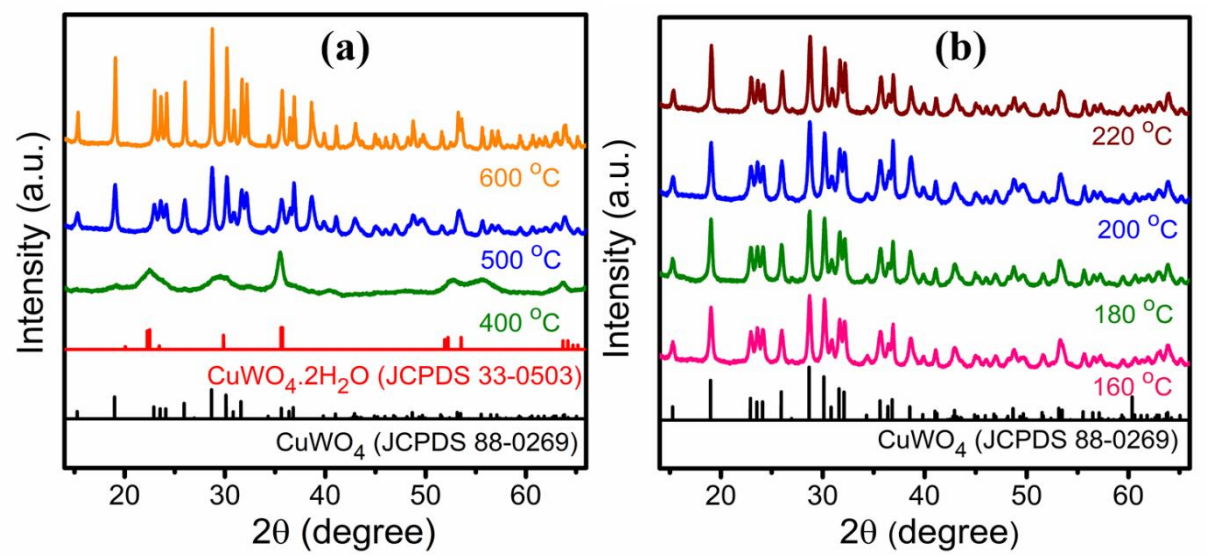


Figure 1. XRD patterns of $CuWO_4$ samples with (a) varying calcination temperatures (CWO-200-y) and (b) varying hydrothermal temperatures (CWO-x-500).

Besides, crystallinity and phase integrity of the samples, prepared at different hydrothermal temperatures and followed by calcination at 500 °C, were investigated and shown in **Figure 1(b)**. Interestingly, all samples calcined at 500 °C consisted of the triclinic $CuWO_4$ structure, with no impurity peaks detected. Specifically, the crystallinity of these samples hydrothermally treated at 160, 180, 200, and 220 °C was calculated to be 93.65, 94.68, 95.15 and 91.58 %, respectively. This indicates that the crystallinity improves as the hydrothermal temperature increases from 160 to 200 °C, reaching its peak at approximately 200 °C. However, as the hydrothermal temperature increases from 200 to 220 °C, the crystallinity decreases. The reduced crystallinity at 220 °C may be attributed to the accelerated reaction rates at this elevated hydrothermal temperature, which lead to uncontrolled growth of $CuWO_4$ crystals. This rapid growth disrupts the formation of well-ordered crystals, resulting in smaller, poorly defined nanoparticles with structure defects, such as vacancies or misalignments [21].

The specific surface area (SSA) and pore structure of the samples were thoroughly analyzed using N_2 adsorption–desorption experiments with the Brunauer Emmett-Teller (BET) method. The SSA of the samples subjected to hydrothermal treatment at (x=) 160, 180, 200 and 220 °C, followed by calcination at 500 °C were found to be 20.3, 18.6, 22.6 and 15.234 m^2g^{-1}, respectively. The corresponding specific pore volumes were 0.042 cm^3g^{-1}, 0.044 cm^3g^{-1}, 0.052 cm^3g^{-1} and 0.07 cm^3g^{-1}. As illustrated in **Figure 2(a)**, all the samples exhibit a typical type-IV according the IPUAC isotherm classification, with an H3-type hysteresis loop (P/P_0 = 0.8 – 1.0), reflecting the existence of primary slit-like mesoporous structure [22, 23]. Additionally, all samples exhibit pore diameters ranging from 1–80 nm, as shown in **Figure 2(b)**, confirming that the samples comprise of micropores, mesopores and macropores. Pores size of all samples falls within the 2–10 nm range, indicating that the pore size is primarily concentrated in the mesoporous region. The mesoporous structure in samples is particularly beneficial for enhancing the adsorption capacity of organic pollutants from wastewater. Variations in SSA and pore size among samples prepared at various hydrothermal temperatures suggest changes in morphology, with a tendency toward increased agglomeration. This agglomeration reduces the SSA, thereby limiting the photocatalytic performance. Nevertheless, the substantial surface area and the well-distributed mesopores are expected to play a significant role in improving the photocatalytic activity of samples.

Considering the crystallinity, phase integrity, SSA, and the dominating mesoporous structure discussed above, the CWO-200-500, synthesized at 200 °C and calcinated at 500 °C, appeared the most attractive from the photocatalytic viewpoint. Its morphology analyzed using FESEM is illustrated in **Figure 2(c)** with noticeable aggregates consisting of almost uniform 55 nm – 100 nm nanoparticles. The zeta-potential of the sample was determined to be –83.9 mV, as shown in **Figure 2(d)**. The point of zero charge (PZC), calculated using Equation (3), was determined to be 8.5. For example, when the medium pH is below 8.5, the surface of CWO-200-500 becomes positively charged, favoring anion adsorption, and vice versa.

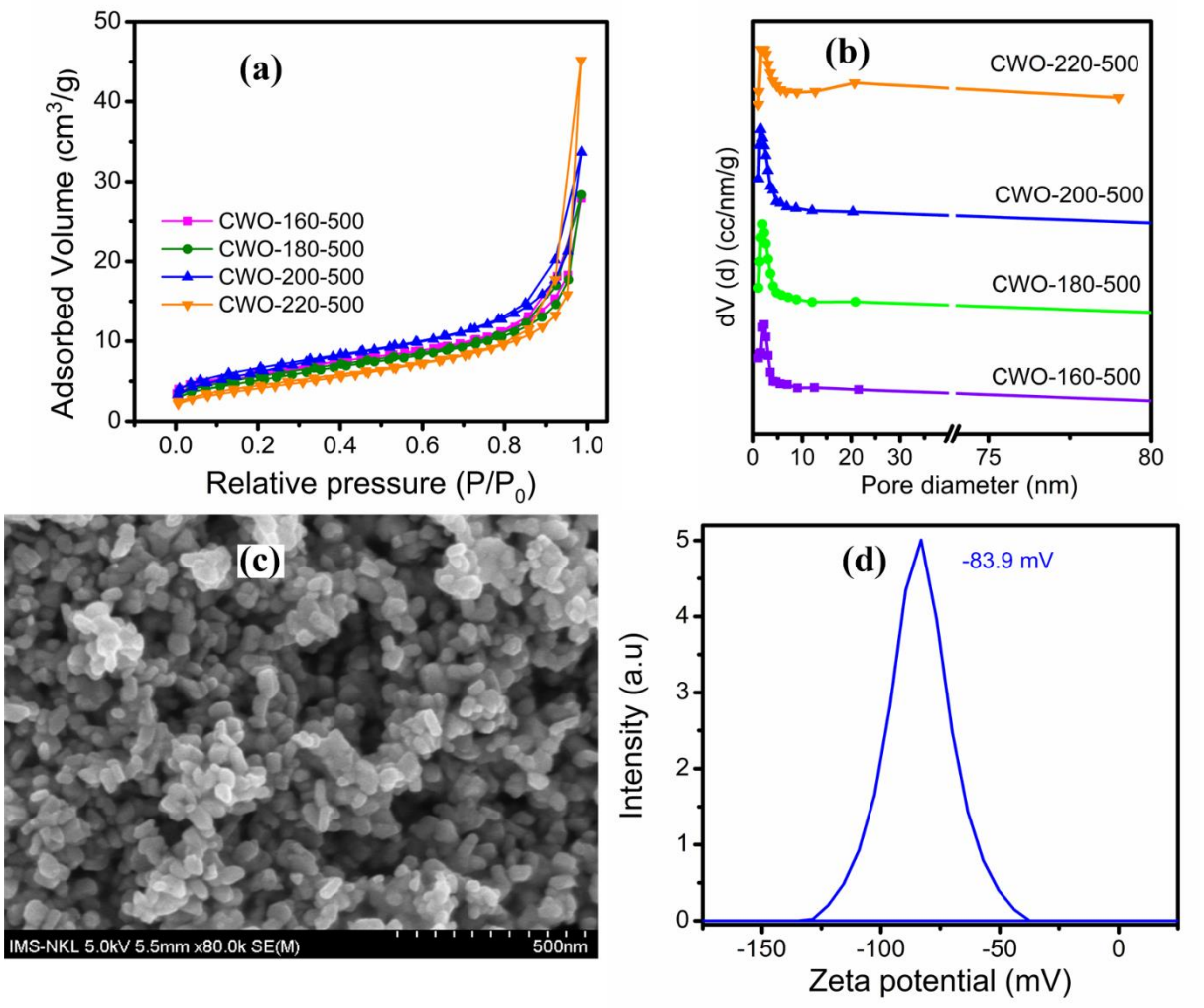


Figure 2. (a) N_2 adsorption-desorption isotherms, (b) BJH pore size distribution, (c) morphology and (d) zeta potential of the CWO-200-500 sample.

Isoelectric Point of Material

The surface charge of the catalyst plays a crucial role in pollutant adsorption and significantly influences its photocatalytic performance. The surface potential of the catalyst can be altered by adjusting the solution's pH. As shown in **Figure 2(d)**, the zeta potential of the sample was measured to be –83.9 mV. Consequently, the pH at PZC (pH_{pzc}) of the material is calculated to be 8.5 using Equation (3). Accordingly, when the pH of the medium is below 8.5, the catalyst surface becomes positively charged, facilitating the adsorption of anions from the solution. Conversely, when the pH exceeds 8.5, the surface acquires a negative charge, which favors the adsorption of cations.

Band gap of the CWO-200-500 sample was calculated by Kubelka-Munk transformation: $(\alpha h\nu)^{1/n} = A(h\nu - E_g)$, where $h\nu$, α, E_g, and A represent the photon energy, absorption coefficient, band gap energy, and arbitrary constant, respectively [24]. The value of n is determined to be 1/2 owing to the direct band gap nature of $CuWO_4$. The band gap value for the sample was determined to be 2.73 eV (as shown in **Figure 3**) which is close to the values in previous researches [25, 26].

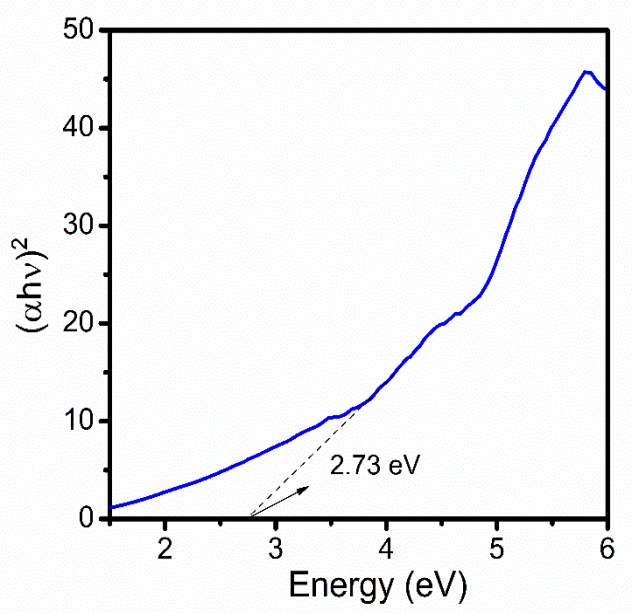


Figure 3. Kubelka-Munk of the CWO-200-500 sample.

Photo-degradation of TC using the Prepared $CuWO_4$

Effect of Hydrothermal Temperature

Photocatalytic activities of samples prepared at different hydrothermal temperatures, followed by calcination at 500 °C, are presented in **Figure 4**. As the hydrothermal temperature increased from 160 to 200 °C, the degradation yield of TC improved (**Figure 4 (a)**), and the pseudo-first-order degradation rate constantly increased from 1.14×10^{-2} min^{-1} to 1.59×10^{-2} min^{-1} (**Figure 4 (b)**). However, the photocatalytic performance decreased sharply when the temperature exceeded 200 °C. At 220 °C, only 81.17% of TC was degraded after 240 min of irradiation, with a corresponding rate constant of 0.83×10^{-2} min^{-1}. The results indicate that the hydrothermal temperature significantly influences the photocatalytic activities of the triclinic $CuWO_4$ phase [27]. The improvement in photocatalytic performance can be attributed to the increase in crystallinity with higher hydrothermally temperatures [28]. The CWO-200-500 sample exhibits the highest visible-light-driven photocatalytic activity, corelating with its highest crystallinity and largest SSA, leading to achieving a 92.35% degradation rate of TC within 3 h. Therefore, a hydrothermal temperature of 200 °C was selected for further analysis.

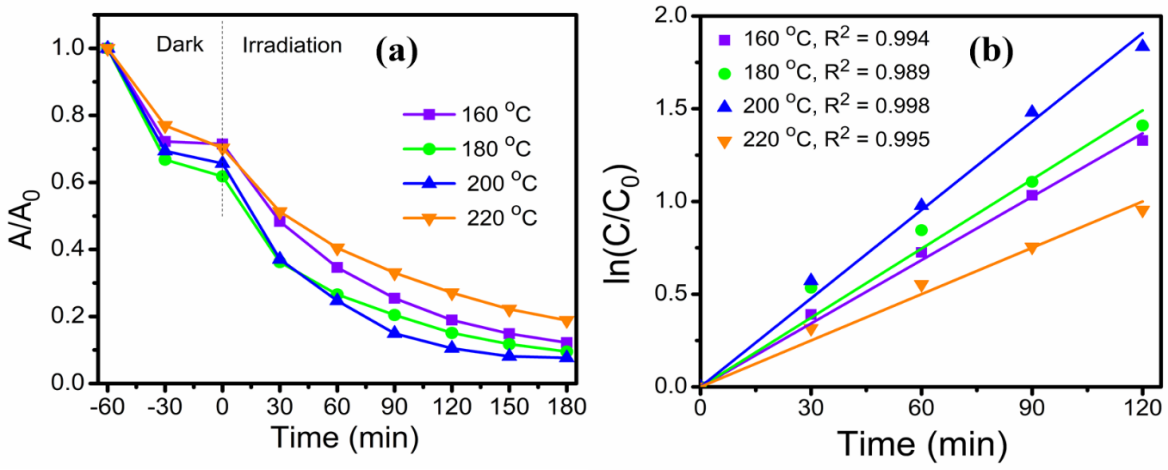


Figure 4. (a) Photocatalytic degradation and (b) kinetic curves of the samples prepared at varying hydrothermal temperatures. Reaction conditions: initial TC concentration 20 mgL^{-1}; photocatalyst dose: 0.5 gL^{-1}, initial pH of TC solution: 4.7.

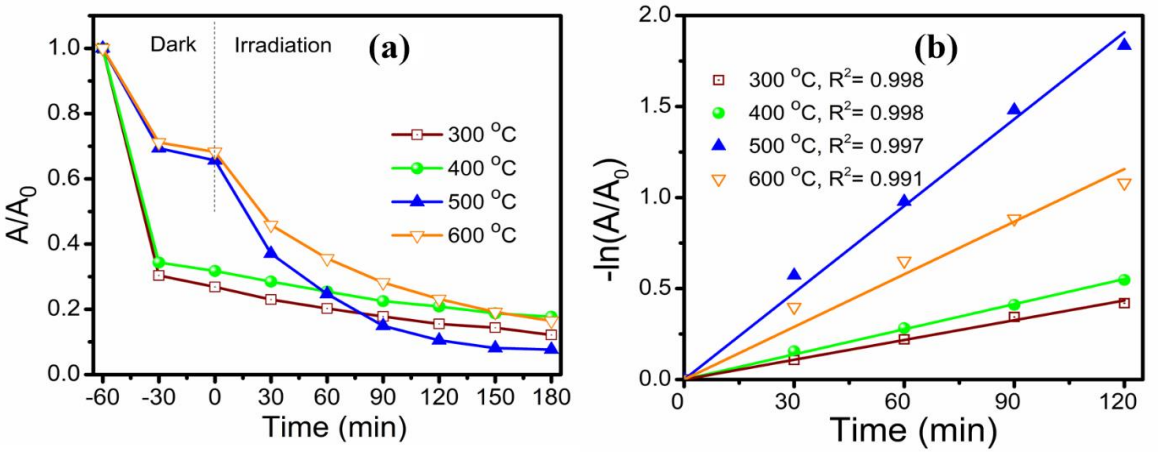


Figure 5. (a) Photocatalytic degradation and (b) kinetic curves of the samples prepared at varying calcination temperatures. Reaction conditions: initial TC concentration 20 mgL^{-1}; photocatalyst dose: 0.5 gL^{-1}, initial pH of TC solution: 4.7.

Effect of Calcinated Temperature

Figure 5 displays the photocatalytic performance of samples prepared hydrothermally at 200 ºC, followed by calcination at various temperatures. Samples which were calcined at 300 °C and 400 °C primarily acted as adsorbents due to the presence of the monoclinic $CuWO_4.2H_2O$ phase, both of which exhibit negligible photocatalytic activity. The higher adsorption performance of these samples can be also attributed to the abundance of hydroxyl functional groups on their surface [9], facilitating greater adsorption capacity. Conversely, as the calcination temperature increases, a phase transition occurs from $CuWO_4.2H_2O$ to the triclinic $CuWO_4$ phase, enhancing the photocatalytic activity for TC degradation. However, further increasing the calcination temperature to 600 °C results in higher crystallinity, which is associated with a reduced SSA, thereby diminishing the photocatalytic efficiency. As a result, the sample prepared at 500 °C achieved 90.5% TC degradation with a pseudo-first-order degradation rate constant of 1.24×10^{-2} min^{-1}.

Effect of Catalytic Dosage on Degradation of TC

Optimizing the photocatalyst dosage is essential not only to maximize degradation rates but also to ensure efficient utilization of catalyst resources. The effect of catalyst dosage on photocatalytic elimination of TC was investigated under specific conditions (initial pH 4.7, TC concentration 20 mgL^{-1}). As illustrated in **Figure 6**, increasing the catalyst dosage from 0.15 gL^{-1} to 0.50 gL^{-1} significantly enhances the elimination of TC. This improvement can be explained by the increase of the available active sites in the solution due to the higher dosage, resulting in the generation of a greater number of reactive radicals responsible for the photocatalytic process [22, 23, 29]. However, in case of the catalyst dosage excess 0.50 gL^{-1}, the TC degradation efficiency increases slightly. This phenomenon may be ascribed to the shielding effect caused by the excessive catalyst particles, which can reduce light penetration and limit photocatalytic efficiency [30]. As a result, the ideal catalyst dosage is selected to be 0.5 gL^{-1} and to be used in further investigations.

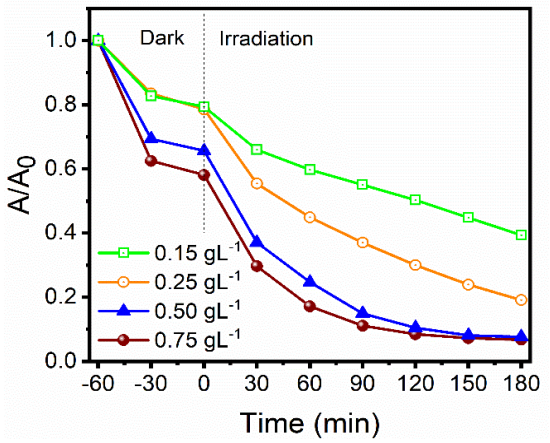
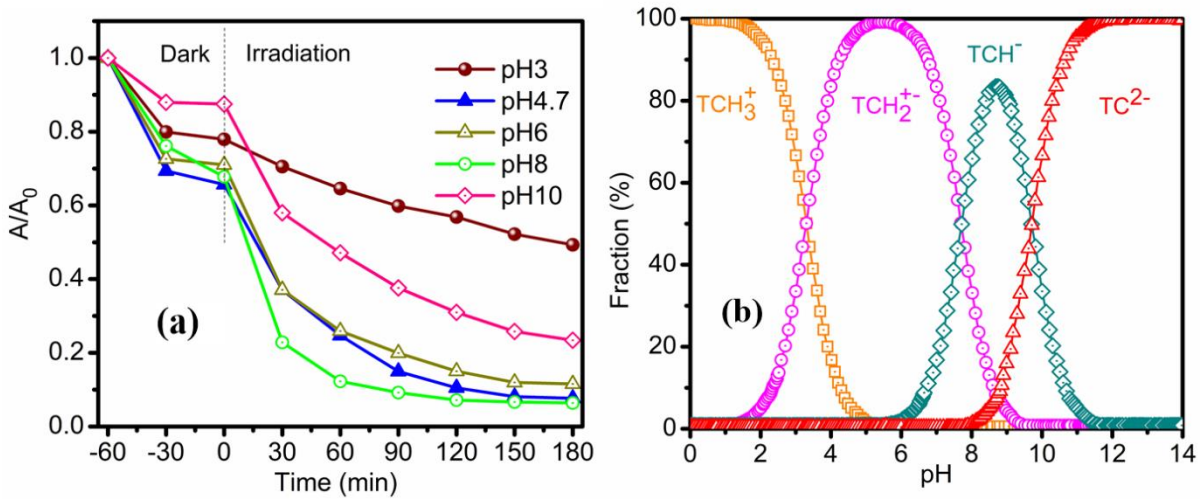


Figure 6. Effect of CWO-200-500 dosage on the TC degradation. Reaction conditions: initial TC concentration 20 mgL^{-1}, initial pH of TC solution: 4.7.

Effect of pH on Degradation of TC

The influence of pH value on the removal efficiency primarily depends on the existence forms of TC molecules in solution, the catalyst surface charge, and the formation of reactive species [31, 32]. In this study, the effect of initial pH of TC solution was studied in the range of pH3–8, with a $CuWO_4$ dose of 0.5 gL^{-1} and initial TC concentration of 20 mgL^{-1}, as displayed in **Figure 7(a)**. It is noted that the original pH of the TC solution (20 mgL^{-1}) was recorded to be 4.7 TC exits in three predominant forms as cation, zwitterion, or anion depending on the pH conditions (as shown in **Figure 7 (b)**) [33]. At a pH value of media below 3.3, TC predominately exists in its TCH_3^+ form, while the catalyst surface also carries a positive charge. This leads to electrostatic repulsion between the TC molecule and the catalyst surface, reducing TC adsorption and consequently lowering the decomposition efficiency. As the pH increases from 3.0 to 7.7 to 8.0, the structures of TC changes progressively from TCH_3^+ to $TCH_2^{\pm}$ (zwitterionic) and then to TCH^- (anionic). Consequently, as the pH of the TC solution increases from 3.0 to 8.0, the positively charged surface of $CuWO_4$ becomes more attractive to the zwitterionic TC molecules. This intensifies the adsorption capacity, leading to an improvement in the TC degradation efficiency of $CuWO_4$. However, when the pH increases further from 8.0 to 10.0, the adsorption capacity of TC by the catalyst decreases. This is due to the electrostatic repulsion between the anionic form of TC (TC^{2-}) and the negative charged catalytic surface, which weakens the adsorption capacity of catalyst [30, 32]. Finally, the appropriate pH for the effective elimination of TC was determined to be pH8, which achieves the highest TC removal efficiency, reaching 93.6%, after 120 min of treatment.



pH value	3.3	7.7	8.5	9.7
TC	TCH_3^+	$TCH_2^{\pm}$	TCH^-	TC^{2-}
Surface charge	+ + + + + +	0	- - - - -	
Electrostatic interaction	Repulsion	Weak	Strong attraction	Repulsion

Figure 7. (a) Effect of initial pH on the TC degradation using CWO-200-500 (initial TC concentration 20 mgL^{-1}; photocatalyst dose: 0.5 gL^{-1}), (b) ionization equilibrium of TC and (c) illustrated the interaction of TC molecule and catalyst surface as a function of solution pH.

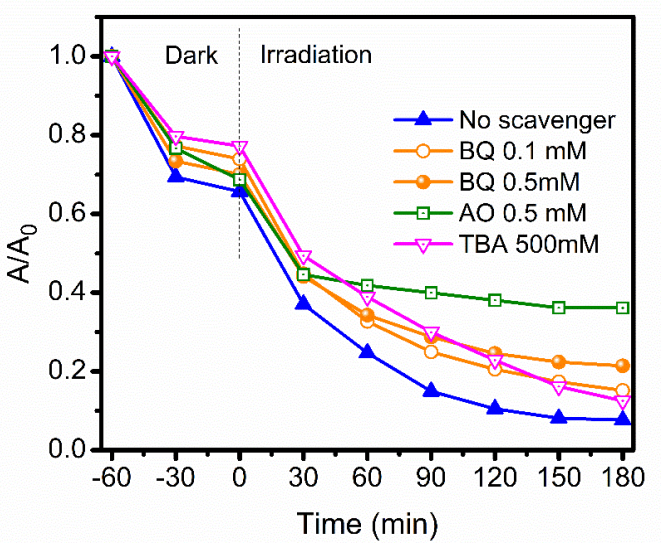


Figure 8. Radical scavenging experiments Reaction conditions: initial TC concentration 20 mgL^{-1}; photocatalyst dose: 0.5 gL^{-1}.

Role of Reactive Species

Under visible light irradiation, the photoinduced electrons and holes are transferred to the surface of the photocatalyst, where they react with the adsorbed water or dissolved oxygen molecules to generate reactive oxygen species (ROS), such as (•OH) and $•O_2^-$. To further confirm the role of these reactive species during the photodecomposition of TC, scavenger experiments were conducted. In each experiment, quencher with specific concentration was added into 200 mL TC solution containing 0.5 gL^{-1} CWO-200-500 catalyst and the pH was maintained at original pH of 20 mgL^{-1} TC (pH4.7). As shown in **Figure 8**, the addition of BQ and TBA as quenchers of $•O_2^-$ and •OH to the reaction solution slightly inhibited TC degradation, with the reaction still maintaining a high rate of approximately 85% after 180 min of treatment, indicating that $•O_2^-$ and •OH play only minor roles in the photocatalysis. In contrast, the degradation of TC was significantly inhibited by the addition of AO, with an inhibition rate of approximately 64 %. These findings indicate that although •OH, $•O_2^-$ and h^+ all contribute to the photocatalytic degradation of TC, h^+ plays a more significant role. This observation aligns with previous studies, which have identified h^+ as the primary reactive species responsible for TC degradation [12, 34, 35]. Based on these results, a mechanism for the degradation of TC by $CuWO_4$ can be proposed as follows:

$$CuWO_4 + h\nu \rightarrow CuWO_4\ (e_{CB}^- + h_{VB}^+) \quad (6)$$

$$e_{CB}^- + O_2 \rightarrow •O_2^- \quad (7)$$

$$h_{VB}^+ + OH^- \rightarrow •OH \quad (8)$$

$$h_{VB}^+ \text{ (major)} + •O_2^- \text{ (minor)} + •OH \text{ (minor)} + TC \rightarrow CO_2 + H_2O + \quad (9)$$

CONCLUSION

The study demonstrates that calcination temperature (400 °C – 600 °C) significantly influences the properties of $CuWO_4$ compared to hydrothermal temperature (160 °C – 220 °C). Among the samples, CWO-200-500, a triclinic phase $CuWO_4$ calcined at 500 °C, exhibited excellent photocatalytic performance, achieving 93.6% degradation of TC within 3 hours under a low-power 26W lamp simulating natural light. This exceptional photocatalytic activity is attributed to its narrow bandgap, large SSA, and high crystallinity, which enhance light absorption and charge separation. The primary reactive species responsible for TC degradation was identified as h^+. Furthermore, the effective use of a low-power light source highlights the potential of CWO-200-500 for efficient water treatment applications, particularly in regions with limited sunlight exposure.

ACKNOWLEDGEMENT

We acknowledge Ho Chi Minh City University of Technology (HCMUT), VNU-HCM for supporting this study.

REFERENCES

1. Al-Alotaibi, A. L., Altamimi, N., Howsawi, E., Elsayed, K. A., Massoudi, I. and Ramadan, A. E. (2021) Synthesis and Characterization of MoO_3 for Photocatalytic Applications. *Journal of Inorganic and Organometallic Polymers and Materials*, **31**, 2017–2029.

2. Niu, Q., Chen, Q., Huang, G., Li, L., He, Y. and Bi, J. (2023) Build-in electric field in $CuWO_4$/covalent organic frameworks S-scheme photocatalysts steer boosting charge transfer for photocatalytic CO_2 reduction. *Journal of Colloid and Interface Science*, **643**, 102–114.

3. Pare, B., Nagraj, G., Solanki, V. S., Albakri, G. S., Alreshidi, M. A., Abbas, M. and Yadav, K. K. (2024) Eco-friendly LEDs radiation-assisted photocatalytic mineralization of toxic azure B dye using Bi_2MoZnO_7 nanocomposite. *Inorganica Chimica Acta*, **568**, 122109.

4. Kavitha, B. and Karthiga, R. (2020) Synthesis and characterization of $CuWO_4$ as nano-adsorbent for removal of Nile blue and its antimicrobial studies. *Journal of Materials and Environmental Science*, **11(1)**, 57–68.

5. López, X. A., Fuentes, A. F., Zaragoza, M. M., Guillén, J. A. D., Gutiérrez, J. S., Ortiz, A. L. and Collins-Martínez, V. (2016) Synthesis, characterization and photocatalytic evaluation of MWO_4 (M= Ni, Co, Cu and Mn) tungstates. *International Journal of Hydrogen Energy*, **41(48)**, 23312–23317.

6. Zhang, C., Zhang, H., Zhang, K., Li, X., Leng, Q. and Hu, C. (2014) Photocatalytic activity of $ZnWO_4$: band structure, morphology and surface modification. *ACS applied materials & interfaces*, **6(16)**, 14423–14432.

7. Aravindraj, K. and Roopan, S. M. (2024) Blue LED assisted indazolone preparation using reusable $CuWO_4$/g-C_3N_5 nanocomposite. *Journal of Photochemistry and Photobiology A: Chemistry*, **115832**.

8. Askari, N., Beheshti, M., Mowla, D. and Farhadian, M. (2020) Synthesis of $CuWO_4$/Bi_2S_3 Z-scheme heterojunction with enhanced cephalexin photodegradation. *Journal of Photochemistry and Photobiology A: Chemistry*, **394**, 112463.

9. Hang, T. T. M., Vy, N. H. T., Hanh, N. T. and Pham, T. D. (2021) Facile synthesis of copper tungstate ($CuWO_4$) for novel photocatalytic degradation of tetracycline under visible light. *Sustainable Chemistry and Pharmacy*, **21**, 100407.

10. Li, D., Yu, X., Tian, N. and Zhang, J. (2024) Oxygen Vacancy induced Strong Interfacial Electric Field for Boosting Photocatalytic Degradation of Tetracycline. *Colloids and Surfaces A: Physicochemical and Engineering Aspects*, **134510**.

11. Liu, P., Sun, M., Xia, S., Ju, J., Mao, W., Zhao, H. and Hao, Y. (2024) Earthworms and lactic acid bacteria (LAB) cooperate to promote the biodegradation of tetracycline residues in livestock manure. *Waste Management*, **186**, 166–175.

12. Chang, L., Pu, Y., Jing, P., Ji, J., Wei, X., Cao, B. and Xie, H. (2022) Z-Scheme $CuWO_4$/BiOCl photocatalysts with oxygen vacancy as electron mediator for boosted photocatalytic degradation of norfloxacin. *Surfaces and Interfaces*, **31**, 102010.

13. Sarwar, A., Razzaq, A., Zafar, M., Idrees, I., Rehman, F. and Kim, W. Y. (2023) Copper tungstate ($CuWO_4$)/graphene quantum dots (GQDs) composite photocatalyst for enhanced degradation of phenol under visible light irradiation. *Results in Physics*, **45**, 106253.

14. Luo, J., Wu, Y., Chen, X., He, T., Zeng, Y., Wang, G. and Chen, Z. (2022) Synergistic adsorption-photocatalytic activity using Z-scheme based magnetic $ZnFe_2O_4$/$CuWO_4$ heterojunction for tetracycline removal. *Journal of Alloys and Compounds*, **910**, 164954.

15. Jatav, N., Shrivastava, A., De, A. K. and Sinha, I. (2022) Experimental and molecular dynamics investigations on Z-scheme visible light Ag_3PO_4/$CuWO_4$ photocatalysts for antibiotic degradation. *Journal of Environmental Chemical Engineering*, **10(3)**, 107975.

16. Schenzel, K., Fischer, S. & Brendler, E. (2005) New method for determining the degree of cellulose I crystallinity by means of FT Raman spectroscopy. *Cellulose*, **12(3)**, 223–231.

17. Hang, T. T. M., Vy, N. H. T., Hanh, N. T. & Pham, T. -D. (2021) Facile synthesis of copper tungstate ($CuWO_4$) for novel photocatalytic degradation of tetracycline under visible light. *Sustainable Chemistry and Pharmacy*, **21**, 100407.

18. Alharthi, F. A., Alanazi, H. S., Alsyahi, A. A. & Ahmad, N. (2021) Hydrothermal synthesis, characterization and exploration of photocatalytic activities of polyoxometalate: Ni-$CoWO_4$ nanoparticles. *Crystals*, **11(5)**, 456.

19. Anucha, C. B., Altin, I., Bacaksız, E., Kucukomeroglu, T., Belay, M. H. & Stathopoulos, V. N. (2021) Enhanced photocatalytic activity of $CuWO_4$ doped TiO_2 photocatalyst towards carbamazepine removal under UV irradiation. *Separations*, **8(3)**, 25.

20. Raizada, P., Sharma, S., Kumar, A., Singh, P., Khan, A. A. P. & Asiri, A. M. (2020) Performance improvement strategies of $CuWO_4$ photocatalyst for hydrogen generation and pollutant degradation. *Journal of Environmental Chemical Engineering*, **8(5)**, 104230.

21. Li, Y., Ding, L., Liang, Z., Xue, Y., Cui, H. and Tian, J. (2020) Synergetic effect of defects rich MoS_2 and Ti_3C_2 MXene as cocatalysts for enhanced photocatalytic H_2 production activity of TiO_2. *Chemical Engineering Journal*, **383**, 123178.

22. Tran, H. T., Ngo, T. H. and Le, M. V. (2024) Metal-free g-C_3N_5 photocatalysts with defect sites as efficient peroxymonosulfate activators for antibiotic removal in aqueous media. *Journal of Environmental Chemical Engineering*, **12(3)**, 112860.

23. Tran, T. H., Ngo, T. H., Oh, W. C. and Le, M. V. (2024) An investigation on the visible light-driven Z-scheme $BiVO_4$/g-C_3N_4 heterostructures: Performance, Evaluation, and Mechanism for Dye and Antibiotics degradation. *Materials Today Communications*, **40**, 109373.

24. Hoang, V. Q. T., Phan, T. Q. P., Senthilkumar, V., Doan, V. T., Kim, Y. S. and Le, M. V. (2019) Enhanced photocatalytic activities of vandium and molybdenum co-doped strontium titanate under visible light. *International Journal of Applied Ceramic Technology*, **16**, 1651–1658.

25. Zhou, S., Wang, Y., Zhao, G., Li, C., Liu, L. and Jiao, F. (2021) Enhanced visible light photocatalytic degradation of rhodamine B by Z-scheme $CuWO_4$/gC_3N_4 heterojunction. *Journal of Materials Science: Materials in Electronics*, **32**, 2731–2743.

26. Bharagav, U., Reddy, N. R., Rao, V. N., Ravi, P., Sathish, M., Shankar, M. V. and Kumari, M. M. (2022) $CuWO_4$ as a novel Z-scheme partner to construct TiO_2 based stable and efficient heterojunction for photocatalytic hydrogen generation. *International Journal of Hydrogen Energy*, **47**, 40391–40406.

27. Souza, E., Sczancoski, J., Nogueira, I., Almeida, M., Orlandi, M., Li, M., Luz, R., Longo, E. & Cavalcante, L. (2017) Structural evolution, growth mechanism and photoluminescence properties of $CuWO_4$ nanocrystals. *Ultrasonics Sonochemistry*, **38**, 256–270.

28. Neto, N. A., Nunes, T., Li, M., Longo, E., Bomio, M. & Motta, F. V. D. (2020) Influence of microwave-assisted hydrothermal treatment time on the crystallinity, morphology and optical properties of $ZnWO_4$ nanoparticles: photocatalytic activity. *Ceramics International*, **46(2)**, 1766–1774.

29. Ngo, T. H., Truong, C. H., Tran, T. H., Luan, V. H., Dang, B. T., Johan, M. R. and Le, M. V. (2024) Development of bismuth-rich bismuth oxyhalides based photocatalyst for degradation of a representative antibiotic under simulated solar light irradiation. *Journal of Photochemistry and Photobiology A: Chemistry*, **446**, 115157.

30. Tran, H. T., Truong, C. H., Ngo, T. H., Dang, B. T., Tseng, T. H., Johan, M. R. and Le, M. V. (2023) The synergy of zinc oxide supported magnetic cobalt ferrite: Efficient boosting the peroxymonosulfate activation towards the refractory organic pollutants elimination. *Journal of Alloys and Compounds*, **968**, 172208.

31. Ravele, M. P., Oyewo, O. A., Ramaila, S., Mavuru, L. and Onwudiwe, D. C. (2021) Photocatalytic degradation of tetracycline in aqueous solution using copper sulfide nanoparticles. *Catalysts*, **11(10)**, 1238.

32. Tang, J., Wang, J., Tang, L., Feng, C., Zhu, X., Yi, Y. and Ren, X. (2022) Preparation of floating porous g-C_3N_4 photocatalyst via a facile one-pot method for efficient photocatalytic elimination of tetracycline under visible light irradiation. *Chemical Engineering Journal*, **430**, 132669.

33. Gopal, G., Alex, S. A., Chandrasekaran, N. and Mukherjee, A. (2020) A review on tetracycline removal from aqueous systems by advanced treatment techniques. *RSC Advances*, **10(45)**, 27081–27095.

34. Yu, X., Li, Z., Liu, Z., Wang, K., Zhang, J. and Yu, Z. (2024) $PbWO_4$ improved the efficient photocatalytic adsorption and degradation of tetracycline and doxycycline by Cu_2O. *Process Safety and Environmental Protection*, **191**, 2725–2746.

35. Chen, J., Yan, Z., Ding, Y., Wang, G. and Xu, Z. (2024) Constructing oxygen defect-rich Bi_2WO_6/CeO_2 S-scheme heterojunction for boosted photocatalytic antibiotic removal. *Chemical Engineering Science*, **287**, 119715.